
Article:
Bonilla Licea, D, Ghogho, M, McLernon, D et al. (1 more author) (2016) Mobility Diversity-Assisted Wireless Communication for Mobile Robots. IEEE Transactions on Robotics, 32 (1). pp. 214-229. ISSN 1552-3098

https://doi.org/10.1109/TRO.2015.2513745

Mobility Diversity-Assisted Wireless Communication for Mobile Robots

Daniel Bonilla Licea, Mounir Ghogho, Des McLernon, Syed Ali Raza Zaidi

***Abstract*—Mobile robots, that wish to communicate wirelessly, often suffer from fading channels. They need to devise an energy efficient strategy to search for a high channel gain position in a near vicinity from which to begin communications. Such a strategy has recently been introduced through the Mobility Diversity with Multi-Threshold Algorithm (MDMTA). In this paper, we establish the theoretical framework for a generalized version of the MDMTA. This allows improved wireless communications in fading channels for mobile robots via intelligent robotic motion with low mechanical energy expenditure.**

***Index Terms*—Autonomous Agents, Robotics Communications, Fading**

I. Introduction

A. Motivation

RECENTLY there has been an increasing interest in robotics communications from both the communications and the robotics communities. In this context some of the problems treated are: how to improve the performance of wireless sensor networks using mobile robots (MRs) [1]; how to take advantage of collaborative communications among numerous mobile robots to find their way out of a maze [2]; how to optimize the position of robotic routers in a wireless robotic network [3], [4] and some other related issues associated with robotic networks [5], [6]; how to optimize the trajectory of a mobile robot to maintain good quality in the communications channel [7], [8]; and finally how to compensate the small scale-fading in wireless channels using the controlled motion of MRs [9], [10], [11], [12], [13]. This last problem is the main topic of this article.

Small-scale fading [14] is a common phenomenon in mobile communications that affects the gain of the wireless channel. It produces random variations in the wireless channel gain across the space. In some cases the fading is so severe that it becomes impossible to communicate. MR communications also suffers from this phenomenon. Therefore in order to make MR communications robust it is necessary to compensate for small-scale wireless channel fading. This can be accomplished through diversity techniques [14].

The idea behind diversity is that due to small-scale fading the channel gain varies randomly across different spatial positions and so the probability that all channels exhibit simultaneously poor gain is lower than the probability that a single channel exhibits poor gain [14]. Diversity techniques construct a new 'artificial channel' by combining[1] multiple channels. In consequence, this 'artificial channel' has a low probability of experiencing a poor gain.

Diversity techniques have been extensively studied and developed in the wireless communications literature for more than fifty years [15] [16], [14]. Classical diversity techniques have been devised for transceivers that are either stationary (e.g., a base station) or whose movement is random and uncontrolled (e.g., a user of a cellular network). But mobile robots, equipped with a wireless transceiver, can both know and control their positions and so this opens the possibility of developing a new class of diversity techniques collectively called 'Mobility Diversity'.

So in summary, the problem tackled in this article is the design of a general intelligent mobility diversity technique to compensate the small-scale fading in wireless channels for MR communications.

B. Problem Overview

From the authors' knowledge, the first articles that mentioned this new form of diversity are [12] and [13]. This technique is known as 'Mobility Diversity' [9], [10], [11], 'RF-Mobility Gain' [12] or simply 'jittery movement' [17], [3]. This technique combats small-scale fading as follows: if the channel gain is poor the MR moves slightly in an intelligent manner to find a position that experiences a better channel. This technique is new, still underdeveloped and the amount of literature dealing with it is very scarce.

In [12] the authors show with real measurements how, in a MR to MR wireless link experiencing small-scale fading, the channel gain can be improved considerably by moving one of the robots a small distance. They show experimentally that this principle actually works. The authors mention that the 'Mobility Gain' principle consists of a searching strategy, a searching goal and a termination criterion. The searching strategies proposed are linear, circular, spiral and random motions. Although the trade-off between the energy used for locomotion and the improvement on the channel gain is mentioned, the authors do not treat the problem of how to optimize the searching space of the MR.

Daniel Bonilla Licea is with the University of Leeds, UK, e-mail:eldbl@leeds.ac.uk. The author acknowledges the funding of CONACYT, Mexico.

Mounir Ghogho is with the University of Leeds, UK and the International University of Rabat, Morocco, e-mail: m.ghogho@ieee.org.

Des McLernon is with the University of Leeds, UK, e-mail: d.c.mclernon@leeds.ac.uk.

Syed Ali Raza Zaidi is with the University of Leeds, UK, e-mail: s.a.zaidi@leeds.ac.uk.

[1]This combination can take different forms. For example averaging all the channels observed (e.g., equal gain combining [16]) or simply selecting the channel with the highest channel gain (e.g., selection combining [16]).

In [13] the authors consider the case in which a MR must follow a predefined trajectory for surveillance purposes and then transmit data to a base station. Real channel measurements were used and the wireless channel presented small-scale fading, in particular Rayleigh fading. The authors show how to modify the trajectory of the MR so that it spends more time in positions with high channel gain and less time in positions with low channel gain, while completing some predefined surveillance trajectory in a certain time.

In section IV-D of [17] the authors propose a "jittery movement" for the MR in order to combat small scale fading. To perform this movement a small circular region around the MR's current position is first defined and then N points are randomly distributed. The MR measures the channel gain at these points and then moves to the one which presents the largest channel gain in order to establish communications.

In [18], the authors show experimentally how a wireless robotic network can improve its performance by compensating small scale fading through micro-movements. The authors propose a distributed algorithm so that each MR explores a number of positions to optimize some networks metrics. The authors consider two different configurations of positions per MR. The first configuration uses two points separated a distance of half wavelength. The second configuration uses five positions where four of them are uniformly arranged into a circle with radius of half wavelength and the fifth position is located at the center of the circle. In practice these configurations produce nearly independent wireless channels but they are not optimized.

Although [12], [13], [17] and [18] present the idea of moving the MR (over a small area) to combat fading there is not a clear understanding about the "optimum" way to move. In our previous work [9] we presented the 'Mobility Diversity with Multi-Threshold Algorithm' (MDMTA) for MRs to combat small-scale fading in wireless links. In this algorithm the MR measures the channel gain over a certain number of stopping points according to some established rules. We also derived the optimum spatial distribution of stopping points for the special cases of $2, 3$ and 4 points, presented a method to determine the optimum number (i.e., 2, 3 or 4) of points to be explored and introduced the concept of 'Adaptive Diversity Order'. We should mention that the MDMTA is a more general case of the simple "jittery movement" proposed in [17].

In all the previous works mentioned the location of the stopping points do not depend on the channel gain observed at previous stopping points but in [10] and [11] the authors proposed adaptive methods to determine the location of the points by using a function of the channel gain observed at previous stopping points. We will refer to these kinds of stopping point geometries presented in [10] and [11] as 'adaptive geometries' while the rest of the geometries will be referred to as 'predetermined geometries'. The disadvantage of 'adaptive geometries' is that they require more knowledge of the wireless channel and thus are computationally more complex and less robust than 'predetermined geometries'. In this article we will focus only on mobility diversity algorithms that use predetermined geometries; the study of adaptive geometries will be the subject of another article.

C. Contribution and Organization

The main component of the MDMTA is the geometry of the points explored by the MR to measure the channel but in the current available literature dedicated to mobility diversity there is not yet a method to optimize the stopping points geometry for an arbitrary number of points. Therefore the main objective of this article is to provide methods to optimize the stopping points geometry for any number of points.

We also mentioned that the MDMTA presented in [9] is a more general case of the algorithm presented in section IV-D of [17], but this is not obvious because the diverse components of the MDMTA have not been properly identified.

The identification and description of the elements composing the MDMTA provides us with a deeper understanding on how this algorithm actually works. This understanding will allow the designer to modify the MDMTA by customizing its existing components or by adding new ones in order to create improved mobility diversity algorithms.

To summarize, the main contributions of this article are:

1) New methods to determine the optimum geometries of any number of stopping points.
2) Formalization of the MDMTA [9] and identification of their components.
3) Optimization methods for the MDMTA parameters.

In section II we describe a realistic model for a particular MR and we also present the model for the wireless channel. In section III we describe the general MDMTA and then show how to optimize it in section IV. Analysis for some simple cases of the MDMTA are developed in section V. Simulation results are presented in section VI and finally conclusions are given in section VII.

II. System Model

A. MR Model

In this article, we consider an omnidirectional MR[2]. In particular we select a three-wheel omnidirectional mobile robot[3] (TOMR) [19]. A TOMR is a MR with three omnidirectional wheels [20], where each wheel is driven by its own motor. The distance from each wheel to the center of the robot is denoted as L. The TOMR model described in this subsection is a version of the model presented in [21]. The robot is equipped with an antenna installed at the geometrical center of the robot (see Fig. 1).

The TOMR position at time t in the global coordinate frame is $\mathbf{p}(t) = [x_g(t) \;\; y_g(t)]^T$ and its pose is $\mathbf{p_o}(t) = [\mathbf{p}(t) \;\; \phi(t)]^T$ where $\phi(t)$ is its orientation. The TOMR pose is related to the control inputs as follows:

$$\begin{aligned} \dot{\mathbf{z}}(t) &= \begin{bmatrix} \mathbf{O}_{3\times3} & \mathbf{I}_{3\times3} \\ \mathbf{O}_{3\times3} & \mathbf{R}(t)\dot{\mathbf{R}}^T(t) - \mathbf{A}^{-1}\mathbf{C} \end{bmatrix} \mathbf{z}(t) \\ &+ \begin{bmatrix} \mathbf{O}_{3\times3} \\ \mathbf{A}^{-1}\mathbf{R}(t)\mathbf{D} \end{bmatrix} \mathbf{u}(t), \end{aligned} \tag{1}$$

[2]An omnidirectional MR can move in any direction at any time.

[3]Although we restrict our analysis to a TOMR the technique presented in this article can be applied to any other type of omnidirectional MR.

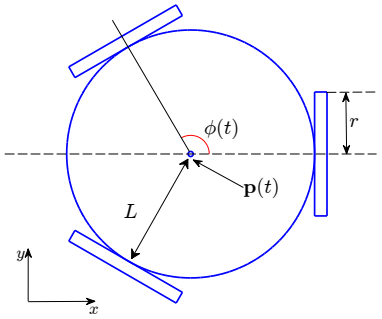

Figure 1. Three-wheeled omnidirectional mobile robot at position $\mathbf{p}(t) = [x_g(t) \;\; y_g(t)]^T$, orientation $\phi(t)$ and with an antenna at its centre.

where $\mathbf{z}(t) = [\mathbf{p_o^T}(t) \;\; \dot{\mathbf{p}}_\mathbf{o}^\mathbf{T}(t)]^T$, $\mathbf{u}(t) = [u_1(t) \;\; u_2(t) \;\; u_3(t)]^T$, $u_i(t)$ is the control input to the ith motor, $\mathbf{O}_{3\times3}$ is a 3×3 zero matrix and $\mathbf{I}_{3\times3}$ is a 3×3 identity matrix. Matrix $\mathbf{A}$ is given by

$$\mathbf{A} = \begin{bmatrix} m + \frac{3J_w}{2r^2} & 0 & 0 \\ 0 & m + \frac{3J_w}{2r^2} & 0 \\ 0 & 0 & J_c + \frac{3J_wL^2}{r^2} \end{bmatrix}, \quad (2)$$

where m is the total mass of the robot, r is the radius of the wheels, L is the distance from the geometric center of the robot to each wheel and J_w and J_c represent the inertia for the robot rotation and for each wheel respectively. We also have $\mathbf{C} = k_1 \text{diag}[1, 1, 2L^2]$, with k_1 being a robot-specific parameter, and the matrix $\mathbf{D}$ is:

$$\mathbf{D} = k_2 \begin{bmatrix} 0 & -\sin(\pi/3) & \sin(\pi/3) \\ 1 & -\cos(\pi/3) & -\cos(\pi/3) \\ L & L & L \end{bmatrix}, \quad (3)$$

where k_2 is another robot-specific parameter. The rotation matrix $\mathbf{R}(t)$ is given by:

$$\mathbf{R}(t) = \begin{bmatrix} \cos(\phi(t)) & -\sin(\phi(t)) & 0 \\ \sin(\phi(t)) & \cos(\phi(t)) & 0 \\ 0 & 0 & 1 \end{bmatrix}, \quad (4)$$

The energy draw from the battery by the MR for motion (we will refer to this as the mechanical energy) from time t_i to t_{i+1} is:

$$\begin{aligned} E_{mech}(t_i, t_{i+1}, \mathbf{u}(t)) &= k_3 \int_{t_i}^{t_{i+1}} \mathbf{u}^T(t)\mathbf{u}(t)dt \\ &- k_4 \int_{t_i}^{t_{i+1}} \dot{\mathbf{p}}_\mathbf{o}^T(t)\mathbf{R}(t)\mathbf{D}\mathbf{u}(t)dt \quad (5) \end{aligned}$$

where k_3 and k_4 are robot-specific parameters. All four parameters (k_1, k_2, k_3 and k_4) depend on various electromechanical parameters of the MR's motors but to avoid introducing more parameters and keep the notation as simple as possible we do not present more details here. The interested reader can find the detailed expression of k_1, k_2, k_3 and k_4 by matching the model presented in [21] to our version.

B. Wireless Channel Model

We consider a communication link between a MR and a stationary node. We assume that there are many scatterers around the MR. This implies that if an electromagnetic wave is radiated by the stationary node's antenna then due to the scatterers there will be many copies of this wave with different angles and different phases arriving at the MR's antenna. These copies combine at the MR's antenna and randomly produce constructive or destructive interference depending on the MR's location. This phenomenon is called small-scale fading or multi-path fading in the communications literature [14]. We also assume that there is neither line of sight between the stationary node and the MR nor a predominant reflected wave. So this particular type of fading is called "Rayleigh fading" [14], as the channel gain has a Rayleigh p.d.f. (probability density function) [14]. Note that this fading is the same type observed in the experimental results of [13]. We also consider that the signals transmitted are narrowband, meaning that their bandwidth is narrow compared to radio frequency carrier of the transmitter. This implies that the wireless channel model is frequency independent. We also assume that the MR's environment is stationary (i.e., it does not change with time during the execution of the mobility diversity algorithm) and so the wireless channel is time invariant (for a given MR position). So taking all the above into account, then the signal received by the MR, when it is located at point $\mathbf{p}(t)$, is:

$$y(t) = s(\mathbf{p}(t)) \cdot h(\mathbf{p}(t)) \cdot x(t) + n(t) \quad (6)$$

where $x(t)$ is the narrowband signal transmitted by the stationary node, $n(t) \sim \mathcal{CN}(0, \sigma^2)$ is[4] the additive white Gaussian noise (AWGN) generated at the MR's receiver. Then $s(\mathbf{p}(t))$ and $h(\mathbf{p}(t)) \sim \mathcal{CN}(0, 1)$ are the shadowing (also known as large-scale fading) [14] and small scale fading terms respectively (both depending on the MR's position, $\mathbf{p}(t)$).The area explored during the execution of the mobility diversity algorithm is small and so we will assume $s(\mathbf{p}(t)) \approx s$. We also assume Jake's model [15] for the multi-path fading and so the channel gain $|h(\mathbf{p}(t))|$ can be considered a bidimensional homogenous and isotropic [22] random scalar field with Rayleigh p.d.f. (standard parameter $\sigma^2 = \frac{1}{2}$) and the following spatial covariance function:

$$\begin{aligned} C_v(\mathbf{p}, \mathbf{q}) &= \frac{\mathbb{E}\left[(H(\mathbf{p}) - \mathbb{E}[H(\mathbf{p})])(H(\mathbf{q}) - \mathbb{E}[H(\mathbf{q})])\right]}{\sqrt{\text{var}(H(\mathbf{p}))\text{var}(H(\mathbf{q}))}}, \\ &= J_0^2\left(2\pi\|\mathbf{p} - \mathbf{q}\|_2/\lambda\right). \quad (7) \end{aligned}$$

where λ is the wavelength used in the radio frequency transmission by the stationary node, $\mathbf{p}, \mathbf{q} \in \mathbb{R}^2$ are any two points on the search space and $H(\mathbf{p}) = |h(\mathbf{p})|$.

III. MDMTA

In this section we discuss the MDMTA. This algorithm combats small-scale fading in a wireless link between a MR and a fixed node[5]. The fixed node uses time division duplex

[4]Note that $\mathcal{CN}(0, \sigma^2)$ means a complex normal random variable with zero mean, variance σ^2 and whose real and imaginary parts are independent and identically distributed.

[5]This node has to remain stationary only during the execution of the MDMTA. So it can be a base station or another MR that remains still during the MDMTA execution.

transmission[6]. During the transmission time the fixed node sends a training signal so that the MR can estimate the channel gain.

The MDMTA is divided into two phases: a searching phase and a selection phase, respectively over the periods $t_1 \leq t < t_N$ and $t_N \leq t \leq t_{N+1}$. During the searching phase the MR stops and estimates the channel gain at N different points called stopping points. By definition the first stopping point $\mathbf{q}_1$ is $\mathbf{p}(t_1)$. If at time instant t_i the estimation of the ith channel gain is greater than the threshold η_i the MDMTA terminates prematurely and the MR then transmits (at point $\mathbf{q}_i$) its data to the stationary node. In this case we will say that the optimum stopping point $\mathbf{q}_{opt}$ is $\mathbf{q}_i$. If the ith channel gain is less than η_i, then the MR moves to $\mathbf{q}_{i+1}$ in $t_{i+1}-t_i$ seconds and repeats the process. If it reaches the Nth stopping point then the searching phase terminates and the selection phase initiates. During the selection phase the MR uses a selection rule ($\mathcal{R}_s$) to determine the optimum stopping point $\mathbf{q}_{opt}$ from which to transmit (the optimum position is not always the one with the highest channel gain as we shall later see) and $H_{opt} = |h(\mathbf{q}_{opt})|$. Then the MR moves from the stopping point $\mathbf{q}_N$ to $\mathbf{q}_{opt}$ in $t_{N+1} - t_N$ seconds.

The MDMTA requires: N, the number of stopping points to be explored; a matrix $\mathbf{Q}_N = [\mathbf{q}_1,\ \mathbf{q}_2, \cdots, \mathbf{q}_N]^T$ containing the positions of the N stopping points to be explored; an $N+1$ dimensional temporal vector $\mathbf{t} = [t_1\ \ t_2 \cdots t_{N+1}]^T$; an $N-1$ dimensional vector $\boldsymbol{\eta} = [\eta_1,\ \eta_2, \cdots,\ \eta_{N-1}]^T$ of thresholds; a selection rule $\mathcal{R}_s$ (to be explained later in this section) and optionally an estimate of the shadowing term s denoted by $\hat{s}$. To simplify notation we will write H_i instead of $H(\mathbf{q}_i)$ in the rest of the article. The pseudocode of the MDMTA is summarized below in Algorithm 1 where $\mathbf{p}$ represents the position of the MR.

Algorithm 1 $MDMTA(N, \mathbf{Q}_N, \mathbf{t}, \boldsymbol{\eta}, \mathcal{R}_s, (\hat{s}))$

1: $\mathbf{p} \leftarrow \mathbf{q}_1$
2: **for** $k = 1$ to $N-1$ **do**
3: $\quad \hat{sH}_k \leftarrow$ Estimate$[sH(\mathbf{p})]$ {Channel gain estimation .}
4: $\quad$ **if** $\hat{H}_k \geq \eta_k$ **then**
5: $\quad\quad$ Terminate Algorithm
6: $\quad$ **end if**
7: $\quad \mathbf{p} \leftarrow \mathbf{q}_{k+1}$ {The MR moves to the next stopping point in $t_{k+1} - t_k$ seconds.}
8: **end for**
9: $\hat{sH}_N \leftarrow$ Estimate$[sH(\mathbf{p})]$
10: $\mathbf{q}_{opt} \leftarrow \mathcal{R}_s$ {A 'selection rule' is used to determine the optimum position.}
11: $\mathbf{p} \leftarrow \mathbf{q}_{opt}$ {The MR moves to the optimum stopping point in $t_{N+1} - t_N$ seconds.}
12: Terminate Algorithm

The thresholds in the MDMTA are used to terminate prematurely the algorithm when the MR finds a stopping point with high channel gain. This is in order to avoid expending more energy by exploring the rest of the stopping points. If the thresholds are too low the probability that $\hat{H}_1 \geq \eta_1$ occurs is high and so the MR will stop most of the time at the first stopping point. This implies that the probability of finding a stopping point exhibiting a high channel gain will be low. On the other hand, if the thresholds are too high then the probability that any channel gain is superior to its corresponding threshold will be considerably low and then the MDMTA will almost never be prematurely terminated, so making the thresholds useless.

Now, as mentioned above, during the execution of the MDMTA the stationary node sends a training signal to the MR. This training signal allows the MR to estimate sH_i (see lines 3 and 9 of Algorithm 1) but the thresholds need to be compared with H_i and not with sH_i (see lines 4 to 6 of Algorithm 1). So the estimation ($\hat{s}$) of the shadowing term[7] is used to obtain $\hat{H}_i$ from the estimation of sH_i for the thresholding (lines 4 to 6 of Algorithm 1).

If the MR does not have an estimate of s and wants to compare η_i directly with sH_i, it would be equivalent to comparing η_i/s with H_i. Since in this case s is unknown, this action would be equivalent to using random thresholds which can be too low or too high (and so having the consequences previously explained). Therefore, if the MR wants to execute the MDMTA but does not know $\hat{s}$, then it would be better to set $\eta_i = +\infty$ to avoid choosing the thresholds too low and so reducing significantly the probability of obtaining a high channel gain. This is why $\hat{s}$ is an optional input parameter for the MDMTA.

The selection rule selects the optimum point ($\mathbf{q}_{opt}$) based on estimates of the product sH_i and so, as opposed to the thresholding issues, it is not necessary to estimate s and H_i separately to implement the selection rule. Nevertheless, for the remainder of the article we will assume that the MR knows $\hat{s}$.

The simplest selection rule $\mathcal{R}_s$ is the *Maximum Channel Gain Rule* which selects the stopping point with the highest estimated channel gain. This selection rule was used in [17] and also in the original MDMTA [9].

Assume that the MR uses the *Maximum Channel Gain Rule*, $\mathbf{q}_{opt} \neq \mathbf{q}_N$ and that $\hat{s}\hat{H}_{opt} = \hat{s}\hat{H}_N + \epsilon$, where ϵ is a small positive number. If this happens, then due to the estimation errors, the following can occur with a non negligible probability. That is, although $\hat{s}\hat{H}_{opt} > \hat{s}\hat{H}_N$, we have in fact $sH_{opt} < sH_N$, which means that the MR would expend energy by moving from $\mathbf{q}_N$ to a stopping point with a lower channel gain ($\mathbf{q}_{opt}$). Now, another possibility is that $sH_{opt} > sH_N$, but the difference is really small and so the MR would expend energy by moving from a $\mathbf{q}_N$ to a stopping point with marginally higher channel gain ($\mathbf{q}_{opt}$).

In order to solve these problems with the *Maximum Channel Gain Rule* we propose a new selection rule: the *Minimum Effort Rule* (see Algorithm 2). The key idea of this new selection rule is to avoid wasting mechanical energy in movement that does not provide a good improvement in the channel gain. So, the MR now moves from $\mathbf{q}_N$ to the point

[6]This means that the fixed node alternates periodically its behaviour acting either as a receiver or a transmitter.

[7]The MR can estimate the shadowing term prior to the MDMTA execution with a technique like the one stated in [23] (implemented by this robot or by a robotic network).

with the highest estimated channel gain only if the difference $((\hat{s}\hat{H}_{k_{max}} - \hat{s}\hat{H}_N)$–see Algorithm 2) is significant, in other words, larger than some threshold μ, see Algorithm 2. Note that if $\mu = 0$ then this selection rule becomes the *Maximum Channel Gain Rule*.

Algorithm 2 $\mathbf{q}_{opt} \leftarrow \mathcal{R}_s(\mu)$ Minimum Effort Rule

1: $k_{max} \leftarrow \arg \max_{k=1,2,\cdots,N-1} \left\{ \hat{s}\hat{H}_k \right\}$
2: **if** $\hat{s}\hat{H}_{k_{max}} - \hat{s}\hat{H}_N > \mu$ **then**
3: $\quad \mathbf{q}_{opt} \leftarrow \mathbf{q}_{k_{max}}$
4: **else**
5: $\quad \mathbf{q}_{opt} \leftarrow \mathbf{q}_N$
6: **end if**
7: return $\mathbf{q}_{opt}$

Now that we have explained in detail the behavior and the components of the MDMTA we will proceed to explain how to optimize this algorithm in the next section.

IV. MDMTA Optimization

First, we will assume that the number of stopping points N is given and then in the last subsection we will show how to optimize it. The general MDMTA optimization problem (MDMTA-OP-1) to be solved is:

MDMTA-OP 1.

$$\begin{aligned} &\min_{\boldsymbol{\eta},\mathbf{t},\mu,\mathbf{Q}_N,\mathbf{u}(t)} f\left(H_{opt}, E_{mech}\left(t_1, t_{N+1}, \mathbf{u}(t)\right)\right) \\ &\text{s.t.} \\ &\mathbf{q}_i \in \mathcal{X}, \quad i = 1, 2, \cdots, N \\ &t_{N+1} - t_1 - T_{max}(N) = 0 \end{aligned} \tag{8}$$

where $\boldsymbol{\eta}$ is the threshold vector, $\mathbf{t}$ is the temporal vector, μ is the *Minimum Effort Rule* input parameter, $\mathbf{Q}_N$ is the matrix describing the geometry of the ordered stopping points (i.e., in the order in which they must be visited), $\mathcal{X}$ is the exploration area[8] in which the stopping points are allowed to lie, $T_{max}(N)$ is a design parameters to limit the maximum execution time of the MDMTA and $f\left(H_{opt}, E_{mech}\left(t_1, t_{N+1}, \mathbf{u}(t)\right)\right)$ is a general cost function (described later in this section) that depends on both the random variable H_{opt} and the mechanical energy spent during the MDMTA execution, i.e., $E_{mech}\left(t_1, t_{N+1}, \mathbf{u}(t)\right)$.

This optimization problem is extremely complicated because it is non-linear, non-convex and it involves the simultaneous optimization of the MDMTA parameters jointly with the geometry of the stopping points (including the order in which they must be visited) and the control law for the MR. A suboptimal but much simpler approach is to partially decouple the optimization of the MDMTA parameters from the optimization of the stopping points geometry, as described in the following subsections.

[8]The exploration area $\mathcal{X}$ must be small enough to ensure that $s(\mathbf{q}_i) = s$ for $i = 1, 2, \cdots, N$.

A. Stopping Points Optimization

The geometry of the stopping points is the main element of the MDMTA. In [9] we presented optimum geometries for two, three and four stopping points. Now, in this section we significantly expand that work by showing how to obtain optimum geometries for any number of stopping points through different procedures.

The stopping points optimization is divided into two subproblems: the geometry optimization, which consists of the optimization of the stopping points' spatial distribution and the visiting order optimization which consists of the optimization of the order in which the stopping points must be visited. We will first discuss the geometry optimization problem and then the visiting order optimization problem.

An omnidirectional MR can traverse any geometry of stopping points in any order always moving in straight line from point to point, but other types of MR may have difficulties in traversing certain geometries. Thus, the omnidirectionality of the TOMR that we are considering in this article allows us to freely design the geometry without incorporating the robot's kinematic constraints [20] into the geometry design.

We present two different approaches to obtain the optimum geometry for the stopping points. In the first approach we restrict the points to lie on a predefined exploration area and then we arrange them in such a way that the expected value of the maximum of the channel gain at all the points is maximized. Mathematically this can be stated as follows:

Geometry-OP 1A.

$$\max_{\mathbf{Q}_N^u} \qquad \mathbb{E}[\max_j H(\mathbf{q}_\mathbf{j}^\mathbf{u})] \tag{9}$$

$$\text{s.t.} \qquad \mathbf{q}_i^u \in \mathcal{X}_e(\rho), \quad i = 1, 2, \cdots, N \tag{10}$$

where $\mathbf{Q}_N^u = [\mathbf{q}_1^u,\ \mathbf{q}_2^u, \cdots, \mathbf{q}_N^u]^T$ is the matrix of unordered stopping points (i.e., this matrix describes the stopping points geometry but it does not indicate the order in which they must be explored). By contrast, $\mathbf{Q}_N$ has the stopping points arranged in the order that they must be visited. Later in this section we will explain how to derive $\mathbf{Q}_N$ from $\mathbf{Q}_N^u$. Note that:

$$\mathcal{X}_e(\rho) = \{[x \quad y]^T \mid x^2 + y^2 \leq \rho^2\}. \tag{11}$$

The solution of this optimization problem depends on the exploration area $\mathcal{X}_e(\rho)$ which in this case was arbitrarily selected to be circular with radius ρ. Other choices are also possible (e.g., a rectangular, elliptic or even a non-convex shape). Note that the exploration area $\mathcal{X}_e(\rho)$ represents the area in which the stopping points can be located and not the area in which the MR can move. A more detailed discussion about the exploration area shape is outside the scope of this article.

Although in general there is no analytical expression for the cost function in $\mathbf{Geometry - OP\ 1A}$, in theory we could use some heuristic optimization algorithm to solve this problem. But due to the lack of an analytical expression for the cost function its true value would have to be estimated via Monte

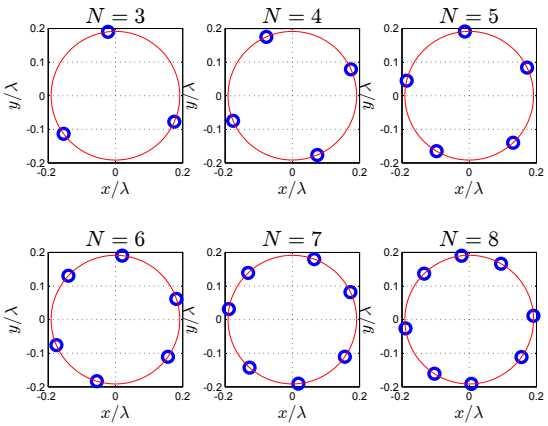

Figure 2. Geometries obtained by solving $\mathbf{Geometry - OP - 1B}$ with $\mathcal{X}_e(0.5z_0)$ using the SA for $N = 3, 4, \cdots, 8$ stopping points.

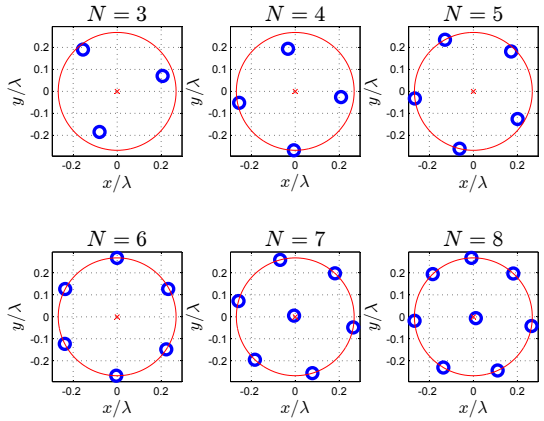

Figure 3. Geometries obtained by solving $\mathbf{Geometry - OP - 1B}$ with $\mathcal{X}_e(0.7z_0)$ using the SA for $N = 3, 4, \cdots, 8$ stopping points.

Carlo simulations. If the variance of the estimation error is not small enough the optimization algorithm could have trouble converging or delivering a reliable solution. To make this variance small enough we need to perform a high number of Monte Carlo simulations to estimate the true value of the cost function thus making the optimization process significantly slow. Therefore, although in theory $\underline{\mathbf{Geometry - OP\ 1A}}$ can be solved, in practice solving this can be problematic, in particular as the number of stopping points N increases.

In order to avoid the aforementioned problems we propose a more tractable approach which consists in minimizing the Frobenius norm of the spatial covariance matrix $\mathbf{C}_N^u$ of the channel gains where the entry of the ith row and jth column is $\mathbf{C}_N^u(i,j) = J_0^2\left(2\pi\|\mathbf{q}_i^u - \mathbf{q}_j^u\|_2/\lambda\right)$. This follows from the fact that as the channel correlation increases the term $\mathbb{E}[\max_j H(\mathbf{q_j})]$ decreases, this is well known in the communications literature [14] and we shall illustrate this in section V-A. The resulting optimization problem is now:

Geometry-OP 1B.

$$\min_{\mathbf{Q}_N^u} \qquad \|\mathbf{C}_N^u\|_F^2 \tag{12}$$

s.t.

$$\mathbf{q}_i^u \in \mathcal{X}_e(\rho), \quad i = 1, 2, \cdots, N \tag{13}$$

where $\|\cdot\|_F$ is the Frobenius norm.

This optimization problem is non-linear, non-convex, with multiple local minima and is $2N$-dimensional (2 variables per stopping point). Antenna array geometry optimization problems [24] have been solved before using the *simulated annealing* (SA) algorithm [25] which is a heuristic searching method. Mathematically, the stopping points geometry problem is a similar problem (although the cost function is different) in the sense that both problems have to determine an optimum distribution of points in the space. Therefore we will also use SA to solve $\mathbf{Geometry - OP\ 1B}$. We have to mention that for $N = 2$ and $N = 3$ both $\mathbf{Geometry - OP\ 1A}$ and $\mathbf{Geometry - OP\ 1B}$ are equivalent.

In Figs. 2 to 5 we observe the geometries obtained by solving $\mathbf{Geometry - OP\ 1B}$ with the SA algorithm for

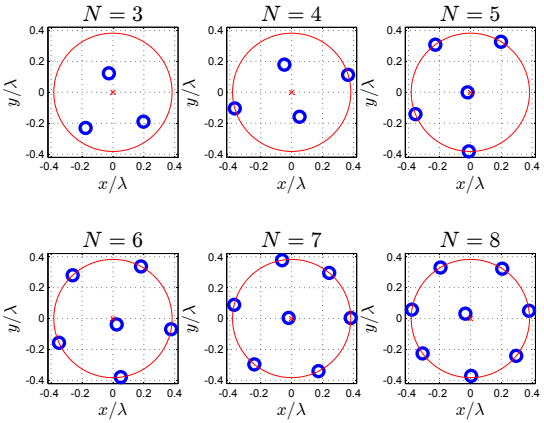

Figure 4. Geometries obtained by solving $\mathbf{Geometry - OP - 1B}$ with $\mathcal{X}_e(z_0)$ using the SA for $N = 3, 4, \cdots, 8$ stopping points.

$N = 3, 4, \cdots, 8$ and with different sizes of the exploration area (i.e., radii of the circles). The SA algorithm aims to find the global solution of the optimization problem through a well designed random search. This implies that in general (in our problem) the geometries obtained by the SA will be very close to the optimum. For example in Fig. 2 for $N = 8$ we observe that the geometry is quite close to a uniform circular array (UCA) and so we may reasonably deduce that the actual optimum geometry is the UCA. This deduction was confirmed by comparing the cost function evaluated with the geometry obtained by the SA with the one evaluated with the UCA geometry.

It is interesting to note that for small exploration areas[9] ($\rho \leq z_0/2$) the optimum geometries (at least for $N \leq 8$) are points on a UCA. But as ρ grows the shape of the optimum geometries changes. The case of $N = 4$ is particularly interesting because the geometry transforms gradually from a perfect square, for small ρ, to a rhombus, for higher values of ρ. This shows that, in general, the shape of the optimum geometries depends on the size of the exploration area. In addition, these results are obtained using a circular exploration

[9] z_0 is the smallest value of z that satisfies $J_0^2(2\pi z/\lambda) = 0$.

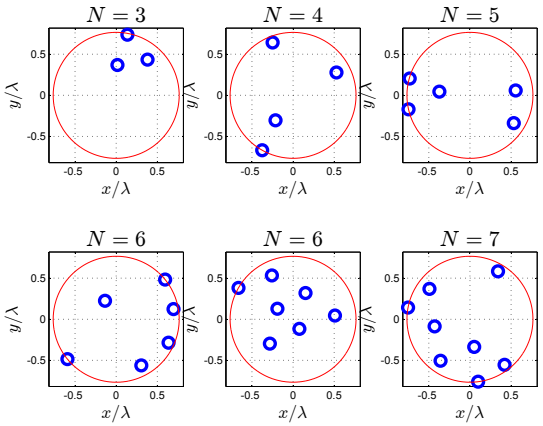

Figure 5. Geometries obtained by solving $\mathbf{Geometry - OP - 1B}$ with $\mathcal{X}_e(2z_0)$ using the SA for $N = 3, 4, \cdots, 8$ stopping points.

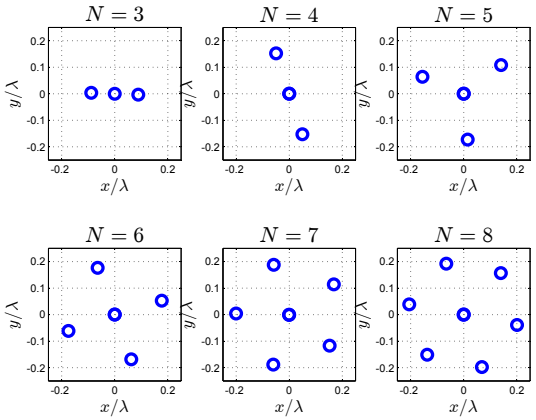

Figure 6. Geometries obtained by solving $\mathbf{Geometry - OP - 2}$ with $\theta = 0.95$ using the SA for $N = 3, 4, \cdots, 8$ stopping points. For $N > 3$ the central circle represents two overlapping points.

area and so if we change the shape of the exploration area (e.g., elliptic or rectangular) the shapes of the optimum geometries may also change. Now, if we observe Fig. 5 we note that the geometries obtained are no longer regular and look more random and spread out. This is because for $\rho \geq z_0$ and a low number of stopping points the number of local minima increases considerably as the exploration area increases. Many of these local minima will have a high value of $\mathbb{E}[\max_j H_j]$ but they will also demand the MR to travel longer distances.

The second approach for deriving optimum geometries consists of arranging the points in such a manner that they provide us with high channel gain while making the points lie as close as possible so that the MR has to move as little as possible. Mathematically this problem can be stated as follows:

Geometry-OP 2.

$$\min_{\mathbf{Q}_N^u} \quad (1-\theta)\|\mathbf{C}_N^u\|_F^2 + \theta \sum_{j=1}^{N} \left(\mathbf{q}_j^u - \frac{1}{N} \sum_{i=1}^{N} \mathbf{q}_i^u \right)^2 \qquad (14)$$

where θ is a design parameter. The cost function minimized in $\mathbf{Geometry - OP\ 2}$ is a convex combination of both the correlation among the channels and the actual spatial spread of the stopping points. Therefore, this cost function will allow us to obtain geometries with channels that have low correlation (i.e., large $\mathbb{E}[\max_j H_j]$), with points that are close together (and so will require a small amount of mechanical energy from the MR while traversing this geometry).

In Figs. 6 to 9 we can see the geometries obtained by solving $\mathbf{Geometry - OP\ 2}$ with the SA algorithm for $N = 3, 4, \cdots, 8$ and different values of θ. In general we can see that the geometries obtained by solving $\mathbf{Geometry - OP - 2}$ and $\mathbf{Geometry - OP\ 1B}$ are different. For high values of θ (see Fig. 6) and $N > 3$ we can observe a curious phenomenon: the optimum geometries have two points overlapping on the center while the remaining $N-2$ points form a UCA. It seems to happen for $N = 8$ and $\theta = 0.9$ (see Fig. 7).

This phenomenon commences when the second term in (14) (i.e., point spatial spread) is very large compared to the first term (i.e., spatial correlation) — i.e., when θ and/or N are

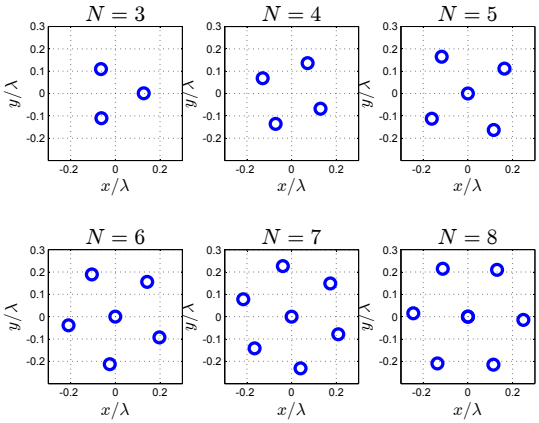

Figure 7. Geometries obtained by solving $\mathbf{Geometry - OP - 2}$ with $\theta = 0.9$ using the SA for $N = 3, 4, \cdots, 8$ stopping points. For $N = 8$ the central circle represents two overlapping points.

too high. The reason for this phenomenon is that under such conditions the point spatial spread term contributes much more to the cost function than the spatial correlation term. Then by overlapping points at the origin the point spatial spread term is considerably reduced and since most of the cost function value is given by this term then the cost function is also considerably reduced even though the spatial correlation is increased. Therefore it is advisable not to use large values of θ in order to avoid this. We should emphasise that if θ is not large enough then the optimum geometries for $N = 3$ and $N = 4$ are the equilateral triangle (as in $\mathbf{Geometry - OP\ 1B}$) and the rhombus geometry (as in $\mathbf{Geometry - OP\ 1B}$ for $\rho > 0.5z_0$). It is interesting to note that the UCA (with an additional extra central point) frequently appears as an optimum geometry for this optimization problem. Finally, we should note that as the number of stopping points N increases and/or the parameter θ decreases it becomes more difficult to solve $\mathbf{Geometry - OP\ 2}$ using the SA algorithm.

It is important to highlight that the geometries shown in Figs. 2 to 9, which are typical cases, can easily be contained into a square of side 2λ. So, given these small dimensions, then along with experimental results relating to the spatial

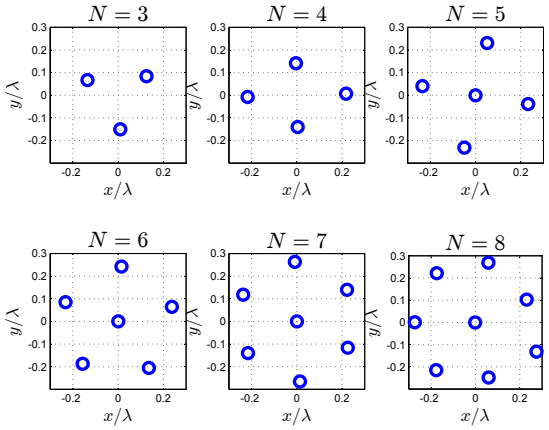

Figure 8. Geometries obtained by solving $\mathbf{Geometry - OP - 2}$ with $\theta = 0.8$ using the SA for $N = 3, 4, \cdots, 8$ stopping points.

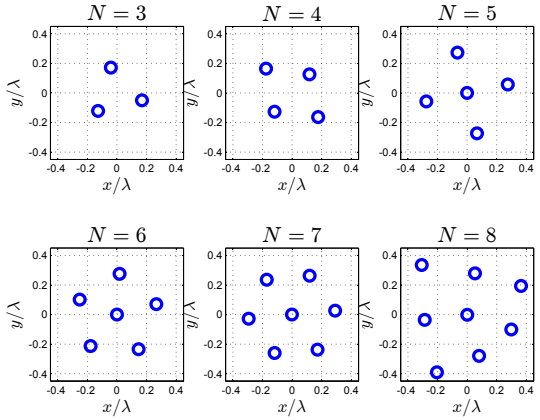

Figure 9. Geometries obtained by solving $\mathbf{Geometry - OP - 2}$ with $\theta = 0.5$ using the SA for $N = 3, 4, \cdots, 8$ stopping points.

autocorrelation function of the shadowing term (s) presented in [26], our assumption that s is approximately constant for all stopping points is clearly justified.

Once we have the optimum matrix[10] $\mathbf{Q}_N^u$ of unordered points we have to establish the optimum visiting order for the stopping points (i.e., the matrix $\mathbf{Q}_N$). A matrix $\mathbf{Q}_N$ is optimum[11] if it minimizes the following cost function:

$$J(\mathbf{Q}_N) = \sum_{k=1}^{N-1} \|\mathbf{q}_{k+1} - \mathbf{q}_k\|_2 + \frac{1}{N} \sum_{j=1}^{N-1} \|\mathbf{q}_j - \mathbf{q}_N\|_2. \quad (15)$$

The first summation on the right hand side of (15) is the distance travelled by the MR while traversing the whole geometry starting at $\mathbf{q}_1$ and finishing at $\mathbf{q}_N$; the second summation is the average distance that the MR needs to travel (after exploring the whole geometry) from $\mathbf{q}_N$ to the point with the highest channel gain. So, the optimum ordering problem can be stated as:

[10]Obtained by solving either $\mathbf{Geometry - OP\ 1B}$ or $\mathbf{Geometry - OP\ 2}$.

[11]Because of the symmetry of the geometries there will be many equivalent orders and thus many equivalent minima.

Ordering-OP.

$$\min_{\mathbf{Q}_N} \quad J(\mathbf{Q}_N) \quad (16)$$

s.t.

$$\mathbf{Q}_N = \mathbf{P}\mathbf{Q}_N^u \quad (17)$$

where $\mathbf{P}$ is a permutation matrix and $\mathbf{Ordering - OP}$ is a combinatorial optimization problem. This problem can easily be solved using "branch and bound [27]" as follows: we first create a tree, where the jth level (the root node is considered the zeroth level) of the tree represents the possible values for $\mathbf{q}_{N+1-j}$ (which are included in $\mathbf{Q}_N^u$). Then we set a bound $\mathcal{B} = +\infty$ (a required parameter for the algorithm [27]) and we explore the leftmost path in the tree until reaching the leaf. Once we reach the leaf we update the value of $\mathcal{B}$ with (15) evaluated along the path explored in the tree. After this, we proceed to explore the next path to the right in the tree. At the jth level of that path we evaluate the partial cost function:

$$J_{BB}(j) = \sum_{k=N+1-j}^{N-1} \|\mathbf{q}_{k+1} - \mathbf{q}_k\|_2 + \frac{1}{N} \sum_{k=N+1-j}^{N-1} \|\mathbf{q}_j - \mathbf{q}_N\|_2. \quad (18)$$

if $J_{BB}(j) \geq \mathcal{B}$ we prune the corresponding subtree and proceed to explore the next path in the tree. If we reach a leaf (i.e., $j = N$) then we update the bound $\mathcal{B} = J_{BB}(N)$ again and explore the next path in the tree. Once we reach the rightmost path the algorithm is terminated and we take as solution the rightmost path that reached a leaf. This method is not necessarily the most efficient way to solve $\mathbf{Ordering - OP}$ but finding the most efficient algorithm to solve it is outside the scope of this article.

We should mention that $\mathbf{Ordering - OP}$ is slightly different from the classical travelling salesman problem in that we are not looking to optimize a tour that starts at $\mathbf{q}_1$, passes through all the stopping points and finishes at $\mathbf{q}_1$ but rather to optimize a path that starts at $\mathbf{q}_1$, passes through all the stopping points until $\mathbf{q}_N$ and then whose finishing position is a random variable uniformly distributed among all the stopping points; the cost function (15) to be minimized is the expected value of the distance travelled during this path.

In Fig. 10 we observe an optimum unordered set of points taken from the optimum matrix $\mathbf{Q}_N^u$ obtained by solving $\mathbf{Geometry - OP\ 1B}$ with the SA for $\mathcal{X}_e(z_0)$ and also we observe the ordered set of stopping points taken from the optimum matrix $\mathbf{Q}_N$. If we do not optimize the permutation matrix and we simply select $\mathbf{P} = \mathbf{I}$ then the MR, when using the MDMTA without thresholds and using *Maximum Channel Gain Rule*, will travel an average distance of $\approx 5.88 z_0$. On the other hand if we optimize $\mathbf{P}$ then the MR, under the same conditions, will travel an average distance of $\approx 4.8 z_0$. In general, by optimizing the visiting order of the stopping points the MDMTA will require the MR to travel smaller distances and so it will be more energy efficient.

Finally, the partial decoupling of the geometry optimization (together with the optimum ordering) from the optimization of the MDMTA parameters allows us to create an 'optimum

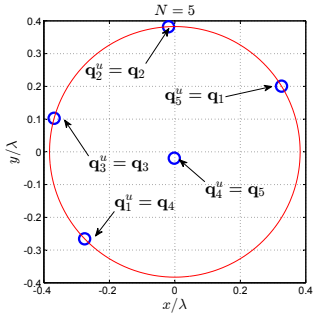

Figure 10. Geometry obtained using the SA with $\mathcal{X}_e(z_0)$ for $N = 5$ stopping points.

geometry dictionary'. This 'optimum geometry dictionary' is indexed by[12] N, ζ and contains at each entry the optimum ordered geometry for those particular parameters. As we will show in the next section, the use of this 'optimum geometry dictionary' can help us to reduce the complexity of the MDMTA optimization.

B. Optimization of the MDMTA parameters

In the preceding subsection we have shown two methods to obtain optimum geometries. Thus we can say that each valid pair of parameters (N,ζ) is associated with a particular optimum geometry. Therefore in this subsection when we refer to a particular geometry optimization problem (either $\mathbf{Geometry-OP\ 1B}$ or $\mathbf{Geometry-OP\ 2}$) and to a valid pair (N, ζ) we are actually referring to a particular optimum geometry.

Now, the optimization of the MDMTA parameters will depend upon the application from which we present two possibilities:

1) An MR wants to transmit a finite amount of data (e.g., pictures, video, measurements or part of a map) consisting of M bits to a stationary node and the bit duration is T_b. The MR uses power control to ensure a reference receive power P_{ref} at the stationary node. In addition the MR cannot radiate more power than P_{max} and if it cannot satisfy P_{ref} at the receiver then it does not transmit at all. In this application the MR uses the MDMTA to minimize the amount of energy used. So, the MDMTA must be optimized to minimize the total amount of energy expended (i.e., the energy used for transmission plus energy used for motion during the MDMTA execution).
2) An MR wants to establish a wireless link with the stationary node to exchange an undetermined amount of data. In this application the MDMTA is used by the MR in the establishment of the wireless link to maximize its signal to noise ratio (SNR). So, in this application the MDMTA is optimized to obtain a good SNR while using as little as possible mechanical energy in the process.

[12]Whether $\zeta = \rho$ or $\zeta = \theta$ depends upon whether we chose $\mathbf{Geometry-OP\ 1B}$ or $\mathbf{Geometry-OP\ 2}$ for the geometry optimization.

In the first application we want to minimize the total amount of energy. If we take into account P_{max} and the outage probability then the statement of the problem becomes more complicated. A simpler approach is to assume $P_{max} = +\infty$ for this optimization. The resulting optimization problem is now:

MDMTA-OP 2.

$$\min_{\boldsymbol{\eta},\boldsymbol{t},\mu,\zeta,\mathbf{u}(t)} \mathbb{E}\left[\frac{\frac{\alpha}{H_{opt}^2} + E_{mech}\left(t_1, t_{N+1}, \mathbf{u}(t)\right)}{\frac{\alpha}{H_1^2}}\right] \quad \text{s.t.} \quad t_{N+1} - t_1 - T_{max}(N) = 0 \tag{19}$$

where $\alpha = \frac{MT_bP_{ref}}{s^2}$, $\boldsymbol{\eta}$ is the threshold vector, $\mathbf{t}$ is the temporal vector, μ is the input parameter for the *Minimum Effort Rule* and ζ is the design parameter for the geometry optimization (i.e., $\zeta = \rho$ if we optimize $\mathbf{Geometry-OP\ 1B}$ and $\zeta = \theta$ if we optimize $\mathbf{Geometry-OP\ 2}$). Inside the expected value of the cost function we have, in the numerator, the total amount of energy that the MR will use if it adopts the MDMTA and, in the denominator, the total amount of energy that the MR will use if it transmits from its initial position and does not use the MDMTA. So, this cost function tells us (on average) how much the energy consumption is decreased by the use of the MDMTA. This optimization problem is a modified and extended version of the optimization problem presented in [9].

Now, the second application can be seen as an investment problem: we want to maximize the revenue (the SNR) while minimizing the investment (the mechanical energy). Therefore, the optimization problem for this application can be stated[13] as:

MDMTA-OP 3.

$$\min_{\boldsymbol{\eta},\boldsymbol{t},\mu,\zeta,\mathbf{u}(t)} (\beta - 1)\mathbb{E}\left[H_{opt}^2\right] + \beta\mathbb{E}\left[E_{mech}\left(t_1, t_{N+1}, \mathbf{u}(t)\right)\right] \quad \text{s.t.} \quad t_{N+1} - t_1 - T_{max}(N) = 0 \tag{20}$$

where $\boldsymbol{\eta}$ is the threshold vector, $\mathbf{t}$ is the temporal vector, μ is the input parameter for the selection rule, ζ is the input parameter for the geometry optimization ($\zeta = \rho$ if we optimize $\mathbf{Geometry-OP\ 1B}$ and $\zeta = \theta$ if we optimize $\mathbf{Geometry-OP\ 2}$) and $\beta \in [0, 1]$ is a design parameter. The cost function is a convex combination of $-\mathbb{E}\left[H_{opt}^2\right]$ with $\mathbb{E}\left[E_{mech}\left(t_1, t_{N+1}, \mathbf{u}(t)\right)\right]$. Therefore, decreasing β means that the improvement in the SNR becomes more important and so the MR is allowed to use more mechanical energy to achieve this goal.

We have to mention that the cost functions of the optimization problems $\mathbf{MDMTA-OP\ 2}$ and $\mathbf{MDMTA-OP\ 3}$ are two different forms of the cost function for the more general optimization problem $\mathbf{MDMTA-OP\ 1}$.

[13]We modelled our problem as an investment problem but we multiplied the cost function by -1 to re-state it as a minimization problem so that all the MDMTA parameter optimization problems in this article are minimization problems.

Now, for both optimization problems, $\mathbf{MDMTA-OP\ 2}$ and $\mathbf{MDMTA-OP\ 3}$, the MR must move from one stopping point to the next one in a finite time $t_{i+1}-t_i$. It is intuitive that in both optimization problems we must use a control law that performs such movements but using minimum energy in order to maximize the energy efficiency of the MDMTA. Therefore the optimum control law $\mathbf{u}(t)$ for $t \in [t_i, t_{i+1}]$ for the TOMR considered in this article is obtained as follows[14]:

Control Law-OP.

$$\begin{array}{l} \min\limits_{\mathbf{u}(t)} E_{mech}\left(t_i, t_{i+1}, \mathbf{u}(t)\right) \\ \text{s.t.} \\ \mathbf{A}\ddot{\mathbf{p}}_o(t) + \mathbf{C}\dot{\mathbf{p}}_o(t) = \mathbf{D}\mathbf{u}(t) \\ \mathbf{p}_o(t_i) = [\mathbf{q}_d^T(i) \quad \phi(0)]^T,\ \mathbf{p}_o(t_{i+1}) = [\mathbf{q}_a^T(i) \quad \phi(0)]^T \\ \dot{\mathbf{p}}_o(t_i) = \mathbf{0}, \quad \dot{\mathbf{p}}_o(t_{i+1}) = \mathbf{0} \end{array} \tag{21}$$

where $i = 1, 2, \cdots, N$, $t_1 = 0$ and $\mathbf{q}_d(i)$ and $\mathbf{q}_a(i)$ are the departure and arrival points at the ith iteration[15]. The cost function corresponds to the mechanical energy consumed by the TOMR, see (5). The first additional condition describes the dynamical model of the TOMR (as described in section II-A) and the remaining restrictions ensure that the TOMR is motionless at both the departure point $\mathbf{q}_d(i)$ and at the arrival point $\mathbf{q}_a(i)$, and it completes the movement in $t_{i+1}-t_i$ seconds.

This is a classical optimum control problem that can be solved analytically using the calculus of variations [28]. The resulting optimum control law for[16] $t \in [t_i, t_{i+1}]$, is given by

$$\mathbf{u}_i^*(t) = \frac{\mathbf{A}_{1,1}\dot{v}_i^*(t) + k_1 v_i^*(t)}{k_2} \begin{bmatrix} \frac{2\sin(\psi_{a,b}(i))}{3} \\ -\frac{\sin(\psi_{a,b}(i))}{3} - \frac{\cos(\psi_{a,b}(i))}{\sqrt{3}} \\ -\frac{\sin(\psi_{a,b}(i))}{3} + \frac{\cos(\psi_{a,b}(i))}{\sqrt{3}} \end{bmatrix} \tag{22}$$

where[17] $\psi_{a,b}(i) = \measuredangle(\mathbf{q}_a(i) - \mathbf{q}_d(i))$ and $v_i^*(t)$ is the optimum translational velocity for $t \in [t_i, t_{i+1}]$ and is given by:

$$\begin{aligned} v_i^*(t) &= \|\mathbf{q}_a(i) - \mathbf{q}_d(i)\|_2 \cdot \left(K_{v1}(\Delta_i) e^{\frac{-t}{\sqrt{\tau}}}\right. \\ &+ \left. K_{v2}(\Delta_i) e^{\frac{t}{\sqrt{\tau}}} + K_{v3}(\Delta_i)\right) \end{aligned} \tag{23}$$

with $\Delta_i = t_{i+1} - t_i$ and:

$$\tau = \frac{2\mathbf{A}_{1,1}^2 k_3}{2k_1^2 k_3 - 3k_1 k_2^2 k_4}, \tag{24}$$

$$\begin{aligned} K_{v_1}(\Delta_i) &= \frac{1 - e^{\frac{\Delta_i}{\sqrt{\tau}}}}{4\sqrt{\tau}\left(1 - \cosh\left(\frac{\Delta_i}{\sqrt{\tau}}\right)\right) + 2\Delta_i \sinh\left(\frac{\Delta_i}{\sqrt{\tau}}\right)}, \\ K_{v_2}(\Delta_i) &= \frac{e^{\frac{-\Delta_i}{\sqrt{\tau}}} - 1}{4\sqrt{\tau}\left(1 - \cosh\left(\frac{\Delta_i}{\sqrt{\tau}}\right)\right) + 2\Delta_i \sinh\left(\frac{\Delta_i}{\sqrt{\tau}}\right)}, \\ K_{v_3}(\Delta_i) &= \frac{2\sinh\left(\frac{\Delta_i}{\sqrt{\tau}}\right)}{4\sqrt{\tau}\left(1 - \cosh\left(\frac{\Delta_i}{\sqrt{\tau}}\right)\right) + 2\Delta_i \sinh\left(\frac{\Delta_i}{\sqrt{\tau}}\right)}. \end{aligned} \tag{25}$$

Therefore, when the optimum control law $\mathbf{u}_i^*(t)$ is used for moving during the ith iteration the mechanical energy consumed over that movement is:

$$E_{mech}\left(t_i, t_{i+1}, \mathbf{u}_i^*(t)\right) = g(\Delta_i)\|\mathbf{q}_a(i) - \mathbf{q}_d(i)\|_2^2 \tag{26}$$

where $g(\Delta_i)$ is given by (27).

Using the optimum control law $\mathbf{u}^*(t)$ and having an 'optimum geometry dictionary' (see subsection IV-A) calculated a-priori, then the searching space of $\mathbf{MDMTA-OP\ 2}$ and $\mathbf{MDMTA-OP\ 3}$ is reduced to $2N$ variables: $\eta_1, \eta_2, \cdots \eta_{N-1}$, $t_2, t_3 \cdots, t_N$, ζ and μ. If we do not dispose of an 'optimum geometry dictionary' then we would have to embed the geometry optimization problem into the optimization of the MDMTA parameters. But this would increase considerably the amount of calculations needed.

If the designer does not have access to the MR model then she/he can replace the mechanical energy term in the cost functions of $\mathbf{MDMTA-OP\ 1}$, $\mathbf{MDMTA-OP\ 2}$ and $\mathbf{MDMTA-OP\ 3}$ with the distance travelled by the MR.

Note that if we want to implement the MDMTA with a non-omnidirectional MR (e.g. a differential drive mobile robot) then the design of the stopping points geometry would have to take into account the kinematic restrictions. In addition, in general the MR could not move in straight line from stopping point to stopping point and probably a joint design of both the optimum stopping points geometry and the minimum energy control law would be necessary. We consider that these modifications are complex enough to constitute the main subject of a future paper and so we will not discuss them in more detail here.

Finally, we have to say that in general there is no analytical expression for the cost functions of $\mathbf{MDMTA-OP\ 1}$, $\mathbf{MDMTA-OP\ 2}$ and $\mathbf{MDMTA-OP\ 3}$ and so the cost function must be calculated by simulations. When calculating the value of the cost function by simulations we will obtain the true value plus a random error (which will be small if we use a large enough number of iterations to calculate it). This makes it more complicated to exactly solve these optimization problems. In this article (see simulation section) we use the SA algorithm to solve these optimization problems, but this does not guarantee us an optimum solution[18] but rather a good or a near optimum solution if we let the SA run for a significant amount of time.

C. Adaptive Diversity Order

We have already shown how to optimize the geometry of the stopping points, the points visiting order and all the parameters

[14] In order to be able to obtain an analytical expression for the optimum control law we restricted the MR so that its orientation remains constant during the whole movement, i.e., $\dot{\phi}(t) = 0$ (see Fig. 1).

[15] At the ith iteration $\mathbf{q}_d(i) = \mathbf{q}_i$, $\mathbf{q}_a(i) = \mathbf{q}_{i+1}$ for $i = 1, 2, \cdots, N-1$, $\mathbf{q}_d(N) = \mathbf{q}_N$ and $\mathbf{q}_a(N) = \mathbf{q}_{opt}$, where $\mathbf{q}_{opt}$ is the optimum point chosen by the selection rule.

[16] We assume that the MDMTA has not been terminated.

[17] $\measuredangle(\mathbf{a})$ represents the angle of the vector $\mathbf{a}$.

[18] This is because the space search is continuous.

$$
\begin{aligned}
g(\Delta_i) &= \left(\frac{2k_3\mathbf{A}_{1,1}^2 - \sqrt{\tau}\mathbf{A}_{1,1}(4k_1k_3 - 3k_2^2k_4) + \tau k_1(2k_1k_3 - 3k_2^2k_4)}{6\sqrt{\tau}k_2^2}\right)\left(1 - e^{\frac{-2\Delta_i}{\sqrt{\tau}}}\right)K_{v_1}^2(\Delta_i) \\
&+ \left(\frac{\mathbf{A}_{1,1}(3k_2^2k_4 - 4k_1k_3) + 2k_1\sqrt{\tau}(2k_1k_3 - 3k_2^2k_4)}{3k_2^2}\right)\left(1 - e^{\frac{-\Delta_i}{\sqrt{\tau}}}\right)K_{v_1}(\Delta_i)K_{v_3}(\Delta_i) \\
&+ \left(\frac{k_1(2k_1k_3 - 3k_2^2k_4)}{3k_2^2}\left(2K_{v_1}(\Delta_i)K_{v_2}(\Delta_i) + K_{v_3}^2(\Delta_i)\right) - \frac{4k_3\mathbf{A}_{1,1}^2}{3k_2^2\tau}K_{v_1}(\Delta_i)K_{v_2}(\Delta_i)\right)\Delta_i \\
&+ \left(\frac{\mathbf{A}_{1,1}(4k_1k_3 - 3k_2^2k_4) + 2k_1\sqrt{\tau}(2k_1k_3 - 3k_2^2k_4)}{3k_2^2}\right)\left(e^{\frac{\Delta_i}{\sqrt{\tau}}} - 1\right)K_{v_2}(\Delta_i)K_{v_3}(\Delta_i) \\
&+ \left(\frac{2k_3\mathbf{A}_{1,1}^2 + \sqrt{\tau}\mathbf{A}_{1,1}(4k_1k_3 - 3k_2^2k_4) + \tau k_1(2k_1k_3 - 3k_2^2k_4)}{6\sqrt{\tau}k_2^2}\right)\left(e^{\frac{2\Delta_i}{\sqrt{\tau}}} - 1\right)K_{v_2}^2(\Delta_i) \qquad (27)
\end{aligned}
$$

of the MDMTA, except for the actual number of stopping points N. In this subsection we address this optimization problem.

The optimization of N prior to each invoking of the MDMTA is called *Adaptive Diversity Order* [9]. The *Adaptive Diversity Order* is one of the elements that differentiates the MDMTA from other diversity techniques in which the diversity order is fixed once the system is deployed (e.g., multi-antenna systems). Now, N is optimized by solving the following problem:

Diversity Order-OP.

$$
\begin{aligned}
&\min_{N} f^*(N, \xi, T_{max}(N)) \\
&\text{s.t.} \\
&T_{max}(N) \leq T_M \\
&N \leq N_{max}
\end{aligned} \qquad (28)
$$

where $\xi = \alpha$ ($\xi = \beta$) if we chose the $\mathbf{MDMTA - OP\ 2}$ ($\mathbf{MDMTA - OP\ 3}$) to optimize the parameters of the MDMTA, $f^*(N, \xi, T_{max}(N))$ denotes the minimum value of the cost function of the optimization problem selected ($\mathbf{MDMTA - OP\ 2}$ or $\mathbf{MDMTA - OP\ 3}$), N_{max} is a predefined maximum value that N may take[19], and $T_{max}(N)$ is the maximum execution time allowed[20] for N stopping points while T_M is the maximum execution time allowed for any number for stopping points.

There are many possible choices for $T_{max}(N)$ but we will only mention two. One option is to set the same duration independently of the number of points $T_{max}(N) = T_M$ and another option is to set the duration proportional to the number of stopping points $T_{max}(N) = \frac{T_M N}{N_{max}}$. The mechanical energy is a decreasing function of $T_{max}(N)$ and since $T_M \geq \frac{T_M N}{N_{max}}$ in general the first option uses less energy while the second option results in a lower MDMTA execution time. So, depending on the particular design requirements we can choose one option or the other.

Now, the minimum value of $T_{max}(N)$ depends on the maximum velocity of the MR, the number of stopping points and the distance between adjacent stopping points. To give a rough idea of typical values of $T_{max}(N)$ for the MDMTA we develop a loose upper bound for its minimum value. As mentioned previously, in typical scenarios the optimum geometries obtained by solving $\mathbf{Geometry - OP\ 1}$ or $\mathbf{Geometry - OP\ 2}$, the distance between adjacent stopping points is in general less than a wavelength λ, see Figs. 2 to 9. If the carrier frequency used is higher than $1\mathrm{GHz}$ then the wavelength is smaller than $30\mathrm{cm}$ and according to the experimental results in [21], the article from which we extracted the TOMR model for this article, this particular MR can at least travel $50\mathrm{cm}$ in one second. Therefore the MR can now move from $\mathbf{q}_N$ to $\mathbf{q}_{opt}$ in less than one second. Now, the time taken for the MR to estimate the channel at each stopping point will depend on the amount of data utilized for this process but in general the time required for this task can easily be assumed less than one second[21]. Considering all this information we can say that the minimum value for $T_{max}(N)$ is loosely bounded by $2N$ seconds: $N-1$ seconds to traverse all the N stopping points, N seconds to measure the channel at all the stopping points and one second to go from $\mathbf{q}_N$ to $\mathbf{q}_{opt}$.

With the introduction of $\mathbf{DiversityOrderOP}$ we have completed the discussion about all the aspects of the MDMTA. In the next section we will analyze the MDMTA in more detail.

V. MDMTA Analysis

A general analysis of the MDMTA is extremely complicated and in most cases it is not possible to obtain analytical results. Nevertheless there are some particular cases of interest in which we can obtain exact analytical expressions for the c.d.f. (cumulative distribution function) of H_{opt} and the p.m.f. (probability mass function) of E_{mech}. These cases are:

1) The MDMTA with two stopping points, using the *Maximum Channel Gain Rule* and assuming perfect channel estimation.
2) The MDMTA with three stopping points, an equilateral triangle geometry with sides of length z_0, using the

[19] A reasonable value for N_{max} can be around 10 or lower.

[20] The actual execution time is a random variable that at most take the value of $T_{max}(N)$.

[21] In this paper for simplicity we are not considering this time but it should be considered when the MDMTA is implemented.

Maximum Channel Gain Rule and assuming perfect channel estimation.

Although we neglected the localization error in this section we analyze how it affects the MDMTA.

A. Two Stopping Points and Perfect Channel Gain Estimation

In this subsection we derive the c.d.f. of H_{opt} and the p.m.f. of E_{mech} for the MDMTA when using the *Maximum Channel Gain Rule* as the selection rule and assuming perfect channel estimation (i.e., the MR measures the channel gain without error). From the MDMTA description we can derive the following expression for the channel gain at $\mathbf{q}_{opt}$:

$$\begin{aligned}\Pr(H_{opt}<x) &= \Pr(H_1<x, H_1\geq\eta_1) \\ &+ \Pr(\max(H_1,H_2)<x, H_1<\eta_1),\end{aligned} \tag{29}$$

where the first probability of the right hand side represents the case where the channel gain at the first stopping point is higher than the threshold η_1 and so $\mathbf{q}_{opt}=\mathbf{q}_1$. The second term represents the case where the MR reaches $\mathbf{q}_2$ and uses the *Maximum Channel Gain Rule* to determine $\mathbf{q}_{opt}$. Doing some probability calculations on (29) we obtain:

$$\begin{aligned}\Pr(H_{opt}<x) &= \Pr(\eta_1\leq H_1<x) \\ &+ \Pr(H_2<H_1<x, H_1<\eta) \\ &+ \Pr(H_1<H_2<x, H_1<\eta)\end{aligned} \tag{30}$$

In order to simplify the analysis we first analyze the c.d.f. for $x<\eta_1$ and then for $x>\eta_1$. For $x<\eta_1$ we have:

$$\begin{aligned}\Pr(H_{opt}<x) &= \Pr(H_2<H_1<x) \\ &+ \Pr(H_1<H_2<x),\end{aligned} \tag{31}$$

and $\Pr(H_2<H_1<x)=\Pr(H_1<H_2<x)$, so

$$\Pr(H_{opt}<x)=2\Pr(H_1<H_2<x). \tag{32}$$

Now, using the integrals from [29], (32) reduces to:

$$\begin{aligned}\Pr(H_{opt}<x) &= 1-e^{\frac{-2x^2}{1-\gamma^2}}I_0\left(\frac{2\gamma x^2}{1-\gamma^2}\right)-2e^{-x^2} \\ &+ 2e^{-x^2}Q_1\left(\frac{\gamma\sqrt{2}x}{\sqrt{1-\gamma^2}},\frac{\sqrt{2}x}{\sqrt{1-\gamma^2}}\right)\end{aligned} \tag{33}$$

where $\gamma=\sqrt{C_v(\mathbf{q}_1,\mathbf{q}_2)}$, see (7). And for $x\geq\eta_1$ we have:

$$\begin{aligned}P(H_{opt}<x) &= P(\eta_1\leq H_1<x) \\ &+ P(H_2<x, H_1<\eta_1)\end{aligned} \tag{34}$$

which again using the integrals from [29] reduces to:

$$\begin{aligned}\Pr(H_{opt}<x) &= 1-2e^{-x^2}+e^{-\eta_1^2} \\ &- e^{-\eta_1^2}Q_1\left(\frac{\sqrt{2}x}{\sqrt{1-\gamma^2}},\frac{\sqrt{2}\gamma\eta_1}{\sqrt{1-\gamma^2}}\right) \\ &+ e^{-x^2}Q_1\left(\frac{\sqrt{2}x\gamma}{\sqrt{1-\gamma^2}},\frac{\sqrt{2}\eta_1}{\sqrt{1-\gamma^2}}\right).\end{aligned} \tag{35}$$

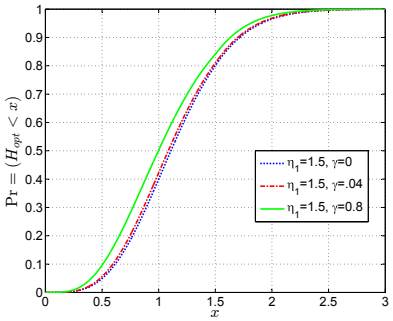

Figure 11. $P(H_{opt}<x)$ for different γ values.

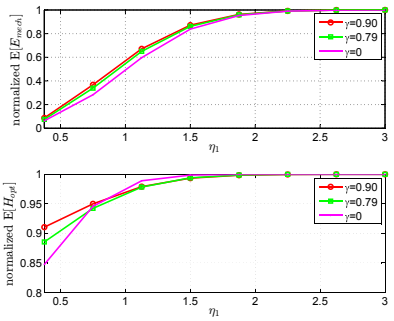

Figure 12. Normalized values for $\mathbb{E}[H_{opt}]$ and $\mathbb{E}[E_{mech}]$ as a function of the threshold η_1 for different γ values and $T_1=T_2$.

The p.m.f. of the mechanical energy consumed by the TOMR when using the optimum control law (22) is:

$$\begin{aligned}&\Pr(E_{mech}=0)=\Pr(H_1\geq\eta_1)=e^{-\eta_1^2} \\ &\Pr(E_{mech}=g(T_1)\|\mathbf{q}_1-\mathbf{q}_2\|_2^2) \\ &=\Pr(H_1<\eta_1,H_2>H_1)=\tfrac{1}{2}\left(1+e^{\frac{-2\eta_1^2}{1-\gamma^2}}I_0\left(\tfrac{2\gamma\eta_1^2}{1-\gamma^2}\right)\right) \\ &-e^{-\eta_1^2}Q_1\left(\tfrac{\gamma\sqrt{2}\eta_1}{\sqrt{1-\gamma^2}},\tfrac{\sqrt{2}\eta_1}{\sqrt{1-\gamma^2}}\right) \\ &\Pr(E_{mech}=(g(T_1)+g(T_2))\|\mathbf{q}_1-\mathbf{q}_2\|_2^2) \\ &=\Pr(H_1<\eta_1,H_1>H_2)=\tfrac{1}{2}\left(1-e^{\frac{-2\eta_1^2}{1-\gamma^2}}I_0\left(\tfrac{2\gamma\eta_1^2}{1-\gamma^2}\right)\right) \\ &+e^{-\eta_1^2}\left(Q_1\left(\tfrac{\gamma\sqrt{2}\eta_1}{\sqrt{1-\gamma^2}},\tfrac{\sqrt{2}\eta_1}{\sqrt{1-\gamma^2}}\right)-1\right).\end{aligned} \tag{36}$$

In Fig. 11 we observe the c.d.f. of H_{opt} for different values of γ. We note that as γ increases then $\Pr(H_{opt}<x)$ increases and it is not difficult to show that $\mathbb{E}[H_{opt}]$ will also reduce. Thus $\mathbb{E}[H_{opt}]$ is maximized when both channels are statistically independent. This result is easily extrapolated to any number of channels and as mentioned in section IV-A it is a well known fact in the communications literature [14].

In Fig. 12 we observe the normalized versions[22] of $\mathbb{E}[H_{opt}]$ and $\mathbb{E}[E_{mech}]$ (calculated from equations (33), (35) and (36)) as functions of η_1. We observe that as η_1 decreases then $\mathbb{E}[E_{mech}]$ reduces more than $\mathbb{E}[H_{opt}]$. This is why we can use the thresholds to slightly reduce $\mathbb{E}[H_{opt}]$ while significantly

[22]The normalization is made with respect to their values when $\eta_1=+\infty$.

reducing the mechanical energy consumption. For example, from Fig. 12, we observe that if $\eta_1 = 1.5$ then $\mathbb{E}[H_{opt}]$ is practically unaffected but $\mathbb{E}[E_{mech}]$ is reduced a little bit more than 10%.

B. Three Stopping Points and Perfect Channel Gain Estimation

In this subsection we derive the c.d.f. of H_{opt} and the p.m.f. of the mechanical energy used considering three stopping points and assuming that the stopping points are arranged in an equilateral triangle geometry with sides of length z_0. This geometry is obtained when we solve $\mathbf{Geometry - OP\ 1B}$ with $\rho = z_0$. In addition, we assume that the MDMTA uses the *Maximum Channel Gain Rule* and that the MR measures the channel gain without estimation error (therefore this analysis represents the best case).

From the algorithm description we have for $x < \min(\eta_1, \eta_2)$:

$$\begin{aligned} \Pr(H_{opt} < x) &= P(\max(H_1, H_2, H_3)) \\ &= (1 - e^{-x^2})^3, \end{aligned} \tag{37}$$

then for $\eta_2 > \eta_1$ and $\eta_1 < x < \eta_2$ we have:

$$\begin{aligned} \Pr(H_{opt} < x) &= \Pr(\eta_1 \leq H_1 < x) \\ &+ \Pr(\max_i(H_i) < x, H_1 < \eta_1) \\ &= e^{-\eta_1^2} - e^{-x^2} \\ &+ (1 - e^{-x^2})^2(1 - e^{-\eta_1^2}), \end{aligned} \tag{38}$$

while for $\eta_1 > \eta_2$ and $\eta_2 < x < \eta_1$ we have:

$$\begin{aligned} \Pr(H_{opt} < x) &= \Pr(\eta_2 \leq H_2 < x, H_1 < \eta_1) \\ &+ \Pr(\max_i(H_i) < x, H_2 < \eta_2) \\ &= (e^{-\eta_2^2} - e^{-x^2})(1 - e^{-\eta_1^2}) \\ &+ (1 - e^{-x^2})^2(1 - e^{-\eta_2^2}), \end{aligned} \tag{39}$$

and finally for $x > \max(\eta_1, \eta_2)$ we have:

$$\begin{aligned} \Pr(H_{opt} < x) &= \Pr(\eta_1 \leq H_1 < x) \\ &+ \Pr(\eta_2 \leq H_2 < x, H_1 < \eta_1) \\ &+ \Pr(\max_i(H_i) < x, \cap_{i=1}^2 H_i < \eta_i) \\ &= e^{-\eta_1^2} - e^{-x^2} \\ &+ (e^{-\eta_2^2} - e^{-x^2})(1 - e^{-\eta_1^2}) \\ &+ (1 - e^{-x^2})(1 - e^{-\eta_1^2})(1 - e^{-\eta_2^2}). \end{aligned} \tag{40}$$

Regarding the p.m.f. of the mechanical energy we have:

$$\begin{aligned} &\Pr(E_{mech} = 0) = \Pr(H_1 \geq \eta_1) = e^{-\eta_1^2} \\ &\\ &\Pr\left(E_{mech} = z_0^2 g(T_1)\right) \\ &= \Pr(H_2 \geq \eta_2, H_1 < \eta_1) = (1 - e^{-\eta_1^2})e^{-\eta_2^2} \\ &\\ &\Pr\left(E_{mech} = z_0^2 \left(g(T_1) + g(T_2)\right)\right) \\ &= \Pr(H_3 \geq \max(H_1, H_2) < x, \cap_{i=1}^2 H_i < \eta_i) \\ &= 1 - e^{-\eta_1^2} - e^{-\eta_2^2} + e^{-\eta_1^2 - \eta_2^2} - (1 - e^{-\min(\eta_1, \eta_2)})^2 \\ &- \tfrac{1}{2}(e^{-\min(\eta_1, \eta_2)^2} - e^{-\max(\eta_1, \eta_2)^2}) \\ &\cdot (1 - e^{-\min(\eta_1, \eta_2)^2}) \\ &+ \int_0^{\min(\eta_1, \eta_2)} \int_0^{\min(\eta_1, \eta_2)} 4xy e^{-2(x^2 + xy + y^2)} dx dy \\ &\\ &\Pr\left(E_{mech} = z_0^2 \textstyle\sum_{i=1}^3 g(T_i)\right) \\ &= \Pr(H_3 < \max(H_1, H_2) < x, \cap_{i=1}^2 H_i < \eta_i) \\ &= (1 - e^{-\min(\eta_1, \eta_2)})^2 \\ &+ \tfrac{1}{2}(e^{-\min(\eta_1, \eta_2)^2} - e^{-\max(\eta_1, \eta_2)^2}) \\ &\cdot (1 - e^{-\min(\eta_1, \eta_2)^2}) \\ &- \int_0^{\min(\eta_1, \eta_2)} \int_0^{\min(\eta_1, \eta_2)} 4xy e^{-2(x^2 + xy + y^2)} dx dy. \end{aligned} \tag{41}$$

We will now attempt to give some interpretation to these mathematical results (in terms of both channel gain and mechanical energy used). Consider two arbitrary positive real numbers a and b with $a > b$. Now, consider two cases: (i)$\eta_1 = a$ and $\eta_2 = b$; (ii) $\eta_1 = b$ and $\eta_2 = a$. We observe from (37) to (40) that for $x > b$ $\Pr(H_{opt} < x)$ is lower in the first case (i) than in the second case (ii). So the first case presents higher $\mathbb{E}[H_{opt}]$ than the second case. And regarding the p.m.f. of E_{mech} we observe from (41) that it is more "skewed" to the left side in case (ii) than in case (i). So the second case presents lower $\mathbb{E}[E_{mech}]$ than the first case. This means that in the MDMTA thresholds selections with $\eta_1 > \eta_2$ will produce higher $\mathbb{E}[H_{opt}]$ but will also consume more mechanical energy than threshold selections with $\eta_1 < \eta_2$. The reason behind this is that in the case with $\eta_1 < \eta_2$ the MR will tend to terminate the MDMTA prematurely in more occasions, move less (lower $\mathbb{E}[E_{mech}]$) and explore less stopping points (lower $\mathbb{E}[H_{opt}]$).

C. Localization Error Impact

In this subsection we briefly discuss the impact of the localization error on the MDMTA. By definition the initial position of the MR is $\mathbf{q}_1$. We assume that the MR uses "dead reckoning [20]" to estimate its relative location to $\mathbf{q}_1$. Then as the MR starts to move from stopping point to stopping point, during the exploration phase the localization error starts to accumulate and so the actual geometry of the stopping points deviates more from the intended geometry as the number of stopping points increases. This is the first effect. Now, during the selection phase, if the jth stopping point was selected as the optimum stopping point then the MR will move believing that it is moving from $\mathbf{q}_N$ to $\mathbf{q}_j$ while in reality it will be moving from $\mathbf{p}(t_N)(\neq \mathbf{q}_N$ due to localization error) to a random point centered at $\mathbf{p}(t_j)$. Note that $\mathbf{p}(t_N)$ is a random variable (centered at $\mathbf{q}_N$) whose variance depends on both the accuracy of the MR motion and the number

Table I
TOMR PARAMETERS

$m = 1.989\text{kg}$	$J_c = 0.020691\text{kg} \cdot \text{m}^2$	$J_w = 0.060\text{g} \cdot \text{m}^2$
$r = 3\text{cm}$	$L = 12.55\text{cm}$	$k_1 = 35.0330\text{N/m}$
$k_2 = 38.7342\text{N}$	$k_3 = 72.9114\text{W}$	$k_4 = 1$

Table II
MDMTA RESULTS FOR THE GEOMETRY $\mathcal{G}_{z_0}(N)$.

N	2	3	4	5
$\mathbb{E}[E_{mech}]$	0.1432	0.2521	0.4221	0.5305
$\mathbb{E}[H^2_{opt}]$	1.4775	1.7944	2.0143	2.1774

of stopping points in the explored geometry. In other words $|h(\mathbf{p}(t_{N+1}))| \neq |h(\mathbf{p}(t_j))|$, and this is the second effect. If the localization error is small then $\mathbf{p}(t_{N+1})$ and $\mathbf{p}(t_j)$ will be close enough, and their channels will be highly correlated and so that $|h(\mathbf{p}(t_{N+1}))| \approx |h(\mathbf{p}(t_j))|$.

Finally we have to mention that as the effects of the localization error accentuate more with the number of stopping points then localization error is one of the elements that (in practice) limits the maximum number (N_{max}) of stopping points that the MR can explore during the MDMTA.

VI. SIMULATIONS

In the simulations, we selected the robot parameters to fit the TOMR used in [21] which describes a real robot. These corresponding parameters are shown in table I. In addition, we will assume throughout this section that the error term in the channel gain estimation has a variance $\sigma_n^2 = 0.05$.

We first compare three different types of geometries:

1) The linear geometry $\mathcal{L}_{z_0}(N)$: In this geometry there are N linear points arranged uniformly spaced at a distance z_0. These points are ordered from left to right.
2) The random geometries $\mathcal{R}_{z_0}(N)$ and $\mathcal{R}_{1.5z_0}(N)$: In these geometries the points are arranged randomly inside a circle of radius z_0 and $1.5z_0$ respectively. The points are not optimally ordered. The random geometries inside a circle to combat fading was suggested in [17].
3) The optimized geometry $\mathcal{G}_{z_0}(N)$: This is obtained by solving $\mathbf{Geometry - OP\ 1B}$ for a circular area of radius $\rho = z_0$. The points are optimally ordered according to $\mathbf{Ordering - OP}$.

In order to compare the geometries we use the MDMTA without thresholds and with the *Maximum Channel Gain Rule*. We assume a wavelength $\lambda = 30\text{cm}$ and $t_{i+1} - t_i = 1\text{s}$ for $i = 1, 2, \cdots, N$.

In tables II to V we observe, for different number of stopping points, the expected value of the mechanical energy spent by the MDMTA for each geometry as well as the power of the optimum channel obtained. We first observe that with the geometry $\mathcal{L}_{z_0}(N)$ we obtain a channel gain with the same characteristics as with $\mathcal{G}_{z_0}(N)$, but using more mechanical energy. The random geometry $\mathcal{R}_{z_0}(N)$ has the same exploration area as $\mathcal{G}_{z_0}(N)$ but provides a poorer channel gain than when using the MDMTA. If the TOMR adopts the geometry $\mathcal{R}_{1.5z_0}(N)$ then it will use more mechanical energy while still obtaining poorer channel gains. Therefore, incorporating an optimum geometry into the MDMTA will allow the MR to obtain good channel gains while using less mechanical energy.

Table III
MDMTA RESULTS FOR THE GEOMETRY $\mathcal{L}_{z_0}(N)$.

N	2	3	4	5
$\mathbb{E}[E_{mech}]$	0.1432	0.3496	0.6186	0.9529
$\mathbb{E}[H^2_{opt}]$	1.4780	1.7812	2.0034	2.1779

Table IV
MDMTA RESULTS FOR THE GEOMETRY $\mathcal{R}_{z_0}(N)$.

N	2	3	4	5
$\mathbb{E}[E_{mech}]$	0.0952	0.1706	0.2404	0.3087
$\mathbb{E}[H^2_{opt}]$	1.3658	1.5818	1.7279	1.8364

Now, we optimize all the parameters of the MDMTA by solving $\mathbf{MDMTA - OP\ 3}$ with $\beta = 0.6$, $T_{max}(N) = N$ and optimizing it assuming the estimation error for the channel gain mentioned at the beginning of this section. The selection rule chosen was the *Minimum Effort Rule*. The results for this optimized algorithm are shown in table VI. Now, if we compare tables II and VI we observe that the power of the optimum channel gain obtained with the optimized algorithm is around 97% to 92% of the one for the non optimized version. But the mechanical energy used by the optimized algorithm is around 50% (and in some cases even 31%) of the one for the non optimized version. Therefore, by choosing the parameter β appropriately we can slightly reduce the channel gain but at the same time significantly reduce the mechanical energy consumption thus making the MDMTA more energy efficient.

Now, we consider the case in which the TOMR must transmit a file of $M = 100\text{MB}$ to the stationary node. The duration of each bit is $T_b = 500\text{ns}$. The MR must satisfy a minimum power of $P_{ref} = 100\mu\text{W}$ at the stationary node receiver and it cannot transmit more than $P_{max} = 40\text{mW}$. We assume that the shadowing term $s = 0.5$ is known. The wavelength used for this transmission is $\lambda = 15\text{cm}$. We optimize the MDMTA with the *Minimum Effort Rule* according to $\mathbf{MDMTA - OP\ 2}$ for $N = 2$ and $T_{max}(2) = 5\text{s}$. By using this optimized MDMTA the outage probability decreases from 10^{-2} to 10^{-3}. In addition, when the communication is successful the energy reduction factor reaches 78%. In other words, when the communication is successful the MR saves 22% of the energy that it would use if it did not employ the MDMTA at all and if $P_{max} = +\infty$. This results show that the MDMTA reduces the outage probability and in the successful communication cases can also reduce considerably the amount of total energy expended (energy used in transmission plus energy used in motion).

Now, we illustrate a possible implementation of the MDMTA in a practical scenario. Consider a robotic wireless network that needs to communicate with a MR in order to

Table V
MDMTA RESULTS FOR THE GEOMETRY $\mathcal{R}_{1.5z_0}(N)$.

N	2	3	4	5
$\mathbb{E}[E_{mech}]$	0.2147	0.3829	0.5393	0.6915
$\mathbb{E}[H^2_{opt}]$	1.4093	1.6598	1.8369	1.9647

Table VI
OPTIMIZED **MDMTA-OP-3** RESULTS.

N	2	3	4	5
$\mathbb{E}[E_{mech}]$	0.0774	0.1274	0.1602	0.1651
$\mathbb{E}[H^2_{opt}]$	1.4470	1.7321	1.9038	2.0055

connect it to the robotic network. To do this a node (another MR) from the robotic network that remains temporally stationary starts to operate in a time division duplex mode. During the transmission period it transmits a training signal to the MR. During the receiving period it waits for an "answer" from the MR. Now, the MR receives this signal but due to small scale fading the received signal has poor SNR. Then it decides to implement the MDMTA to improve the quality of the wireless link before answering to the stationary node. To avoid making the stationary node wait too long the designer sets in the MR's program the time limit $T_M = 5$ seconds. The MR has in memory a number of geometries of different sizes and a different number of stopping points (up to $N = 5$) optimized according to $\mathbf{Geometry - OP\ 1B}$ and $\mathbf{Ordering - OP}$. The MR also has in memory two preloaded tables containing the optimum parameters of the MDMTA according to $\mathbf{MDMTA - OP\ 3}$. It will also have the corresponding value of the cost function for up to $N = 5$ stopping points and different values of the parameter β. The first preloaded table has the optimum parameters of the algorithm using the thresholds $\eta_i = +\infty$, while the second preloaded table gives the optimum value of all the parameters including the thresholds. If the MR's battery is almost full, and establishing communication with the robotic network is very important, it will select β small to prioritize finding a large channel gain (as opposed to expenditure of mechanical energy, see (20)). Now, in order to apply the adaptive diversity mechanism it first realizes that in this particular case it does not have an estimate of the shadowing term (s) and so it explores all the entries of the first table having small β and then selects the row with the lowest cost function value. Then the MR reads that row, picks the values for all its parameters and executes the MDMTA according to Algorithm 1. Finally, when it reaches $\mathbf{q}_{opt}$ it communicates with to the robotic network.

VII. CONCLUSIONS

We have generalized the MDMTA and we have provided two different answers in relation to what an optimum search geometry actually means. We have shown how to obtain this geometry for any number of stopping points. We showed that there are different possibilities as regards defining the optimization problem for the MDMTA when searching the optimum channel gain and these depend on the particular application. We also highlighted the importance of optimizing the search geometry as well as the parameters of the MDMTA in order to make the algorithm more (mechanical energy) efficient when searching for the optimum channel gain. So in summary, we have developed the theory for a new generalized MDMTA, verified its advantages via simulation and analytical results, and laid the foundations for future intelligent/energy efficient mobility diversity algorithms.

This paper shows how to design the optimum geometries for omnidirectional MRs. In future work we will extend the problem of designing the stopping point geometries to non-omnidirectional MRs which take into account their kinematic constraints. Furthermore, instead of using predetermined geometries as with in this paper, it could be possible to create a technique to determine adaptively the best position of the next stopping points based on the knowledge of the channel at previous stopping points, their spatial correlations and the position of near obstacles. Finally, we considered the case of a single wireless link and so this technique can be extended to consider multiple wireless links thus making this method more appealing for an application in robotic wireless networks.

VIII. REFERENCES

REFERENCES

[1] X. Li, R. Falcon, A. Nayaak and I. Stojmenovic, "Servicing Wireless Sensor Networks by Mobile Robots", IEEE Communications Magazine, vol 50., no. 7, July 2012.

[2] J. H. Jung, S. Park and S. Kim, "Multi-Robot Path Finding with Wireless Multihop Communications", IEEE Communications Magazine, vol 48., no. 7, July 2010.

[3] Y. Yan and Y. Mostofi, "Robotic Router Formation in Realistic Communication Environments", IEEE Transactions on Robotics, vol. 28, no. 4, August 2012.

[4] S. Gil, S. Kumar, D. Katabi, D. Rus, "Adaptive Communication in Multi-Robot Systems Using Directionality of Signal Strength", Proc. of the International Symposium on Robotics Research, 2013.

[5] M.M. Zavlanos, A. Ribeiro and G. J. Pappas, "Network Integrity in Mobile Robotic Networks", IEEE Transactions on Automatic Control, vol. 58, no. 1, January 2013.

[6] R.K. Williams, A. Gasparri and B. Krishnamachari, "Route Swarm: Wireless Network Optimization through Mobility", Proc. of International Conference on Intelligent Robots and Systems (IROS), 2014.

[7] C. C. Ooi and C. Schindelhauer, "Minimal energy path planning for wireless robots", Mobile Networks and Applications, vol. 14, no. 3, January. 2009.

[8] A. Ghaffarkhah and Y. Mostofi, "Communication-Aware Motion Planning in Mobile Networks", IEEE Transactions on Automatic Control, vol. 56, no. 10, October 2011.

[9] D. Bonilla Licea, D. McLernon, M. Ghogho and S. A. Raza Zaidi, "An Energy Saving Robot Mobility Diversity Algorithm for Wireless Communications", Proc. of the 21st European Signal Processing Conference (EUSIPCO), 2013.

[10] D. Bonilla Licea, D. McLernon and M. Ghogho,"A mobility diversity algorithm with Markovian trajectory planners", Proc. of the 23rd IEEE International Workshop on Machine Learning for Signal Processing (MLSP), 2013.

[11] D. Bonilla Licea, D. McLernon and M. Ghogho,"Designing Optimal Trajectory Planners for Robotic Communications", Proc. of the 1st IET Intelligent Signal Processing (ISP) conference, 2013.

[12] J. M. Smith, M. P. Olivieri, A. Lackpour and N. Hinnerschitz, "RF-mobility gain: concept, measurement campaign, and explotation", IEEE Wireless Communications, vol. 16, no. 1, February 2009.

[13] M. Lindhe and K. H. Johansson, "Using robot mobility to exploit multipath fading", IEEE Wireless Communications, vol. 16, no. 1, February 2009.

[14] A. Goldsmith, *Wireless Communications*, Cambridge University Press, 2005.

[15] W.C. Jakes, *Microwave Mobile Communications*, Wiley. IEEE Press, 2011.

[16] M. K. Simon, M. Alouini, *Digital Communication over Fading Channels*, 2nd Edition, Wiley-IEEE Press, 2005.

[17] A. Ghaffarkhah and Y. Mostofi, "Path planning for networked robotic surveillance", IEEE Transactions on Signal Procesing, vol. 60, no. 7, July 2012.
[18] Vieira, Marcos A.M. et al., "Mitigating multi-path fading in a mobile mesh network", Ad Hoc Networks, vol. 11, no. 4, June 2013, pp 1510 - 1521.
[19] S. G. Tzafestas, *Introduction to Mobile Robot Control*, Elsevier, 2014.
[20] R. Siegwart., I.R. Nourbakhsh and D. Scaramuzza, *Introduction to autonomous mobile robots*, MIT Press, 2011.
[21] H. Kim, B.K. Kim ,"Minimum-energy trajectory planning and control on a straight line with rotation for three-wheeled omni-directional mobile robots", Proceedings of the IEEE/RSJ International Conference on Intelligent Robots and Systems (IROS), 2012, pp 3119 - 3124.
[22] D. R. Brian, *Spatial Statistics*, Wiley Series in Probability and mathematical statistics.
[23] M. Malmirchegini and Y. Mostofi, "On the Spatial Predictability of Commucation Channels", IEEE Transactions on Wireless Communications, vol. 11, no. 3, March 2012.
[24] P. J. Bevelacqua and C. A. Balanis, "Optimizing Antenna Array Geometry for Interference Suppression", IEEE Transactions On Antennas And Propagation, vol. 55, no. 3, March 2007.
[25] S. Russell, P. Norving, *Artificial Intellingence: A Modern Approach*, Prentice Hall, 2003.
[26] A. Algans, K. I. Pedersen and P. E. Mgensen, "Experimental Analysis of the Joint Statistical Properties of Azimuth Spread, Delay Spread, and Shadow Fading", IEEE Journal on Selected Areads in Communications, vol. 20, no. 3, April 2002.
[27] B. Korte and J. Vygen, *Combinatorial optimization: Theory and algorithms*, 4th Edition, Springer, 2008.
[28] D. E. Kirk, *Optimal control theory: An introduction*. Dover Publications, Inc., 2004.
[29] A. H. Nuttall, "Some integrals involving the Q-function" Naval Underwater Systems Center (NUSC) technical report, April 1972.

Daniel Bonilla Licea received his telematics engineering degree from the Unidad Profesional Interdisciplinaria en Ingenieria y Tecnologias Avanzadas, UPIITA, Mexico, in 2009. He received his M.Sc. degree in communications from the Centro de Investigacion y Estudios Avanzados, CINVESTAV, Mexico City, in 2011. From May 2011 until June 2012, he did an internship in the signal processing team of Intel Labs in Guadalajara, Mexico. From September 2012 to the present day he has been doing a PhD at the School of Electronics and Electrical Engineering, University of Leeds, U.K.

Syed Ali Raza Saidi received his B.Eng.degree in information and communication system engineering from the School of Electronics and Electrical Engineering, NUST, Pakistan, in 2008. He was awarded the NUST most prestigious Rector's gold medal for his final year project. From September 2007 until August 2008, he served as a Research Assistant in the Wireless Sensor Network Lab on a collaborative research project between NUST, Pakistan, and Ajou University, South Korea. In 2008, he was awarded the overseas research student (ORS) scholarship along with the Tetley Lupton and Excellence Scholarships to pursue his Ph.D. at the School of Electronics and Electrical Engineering, University of Leeds, U.K. He was also awarded with the COSTIC0902, DAAD, and Royal Academy of Engineering grants to promote his research. His research is focused on the design and analysis of large scalead-hoc wireless networks by employing tools from stochastic geometry and random graph theory.

Des McLernon received his B.Sc in electronic and electrical engineering and his M.Sc. in electronics, both from Queen's University of Belfast,N. Ireland. He then worked on radar research and development with Ferranti Ltd. in Edinburgh, Scotland, and later joined the Imperial College, University of London, where he received his Ph.D.in signal processing. After first lecturing at South Bank University, London, UK, he moved to the School of Electronic and Electrical Engineering at the University of Leeds, UK, where he is a Reader in Signal Processing. His research interests are broadly within the domain of signal processing for communications, in which area he has published over 280 journal and conference papers.

Mounir Ghogho Mounir Ghogho received the PhD degree in 1997 from the National Polytechnic Institute of Toulouse. Since 2001, he has been a full Professor with the EEE school of the University of Leeds (UK). Since 2010, he has also been affiliated with the International University of Rabat. He is an Associate Editor of the IEEE Signal Processing magazine. He previously served as Associate Editor of IEEE Transactions on Signal Processing. He is a member of the IEEE SAM Technical Committee. He was awarded the UK Royal Academy of Engineering Research Fellowship in 2000 and the 2013 IBM Faculty award in 2013.